Received: 18 April 2021 | Revised: 19 June 2021 | Accepted: 3 July 2021

DOI: 10.1111/jfpe.13814

ORIGINAL ARTICLE

Journal of Food Process Engineering WILEY

Poly(3-hydroxybutyrate-co-3-hydroxyhexanoate) with zinc oxide nanoparticles for food packaging

Ana M. Díez-Pascual

Universidad de Alcalá, Facultad de Ciencias, Departamento de Química Analítica, Química Física e Ingeniería Química, Ctra. Madrid-Barcelona, Km. 33.6, 28805 Alcalá de Henares, Madrid, Spain

Correspondence
Ana M. Díez-Pascual, Universidad de Alcalá, Facultad de Ciencias, Departamento de Química Analítica, Química Física e Ingeniería Química, Ctra. Madrid-Barcelona, Km. 33.6, 28805 Alcalá de Henares, Madrid, Spain.
Email: am.diez@uah.es

Abstract

Poly(3-hydroxybutyrate) (PHB) is a biodegradable biopolyester synthesized via bacterial fermentation from renewable resources that has received great attention over the last years for medicine and food packaging applications. However, it shows several shortcomings such as narrow processing window and a high crystallinity (>50%), which leads to brittleness and low impact resistance. To solve these drawbacks, the hydroxybutyrate units can be copolymerized with other monomers like 3-hydroxyhexanoate to yield poly(3-hydroxybutyrate-co-3-hydroxy-hexanoate) (PHBHHx), a copolymer with higher ductility, improved impact strength, and lower melting point. However, PHBHHx displays lower crystallinity than PHB, hence reduced stiffness, and poorer barrier properties against moisture and gases, which is a disadvantage for its use as food packaging material. In this regard, (PHBHHx)-based bionanocomposites incorporating 0.5, 1.0, 2.0, and 5.0 wt% zinc oxide (ZnO) nanoparticles were synthesized via solution casting technique. Their morphology, mechanical, thermal, barrier, and antibacterial properties were investigated via transmission electron microscopy, tensile and impact strength tests, thermogravimetric analysis, water vapor, and oxygen permeability measurements as well as antibacterial tests. In terms of gas permeability, the optimum performance was attained at 5.0 wt % ZnO loading, with reductions in the water vapor and oxygen permeability of 45 and 33%, respectively. Conversely, the impact strength decreased with increasing ZnO concentration, leading to 25% reduction for the highest ZnO loading tested. The bionanocomposite with 5.0 wt% ZnO is a promising alternative to synthetic plastics, with an optimal balance of toughness, barrier, and antibacterial properties to be used in packaging and disposable applications such as beverage and food containers.

Practical applications

This study analyzes the morphology, thermal, mechanical, barrier, and antibacterial properties of biodegradable nanocomposites based on PHBHHx copolymer and ZnO nanoparticles. These safe and environmentally friendly nanomaterials can be used as a sustainable alternative to synthetic plastics for food and beverage containers.

1 | INTRODUCTION

Over the past decades, the amount of plastics used in food packaging applications has extraordinarily increased. Thus, numerous synthetic polymers derived from non-renewable resources such as polypropylene (PP), polystyrene (PS), polyethylene terephthalate (PET), and polyvinylchloride (PVC) have been frequently applied in food packaging. This issue has raised many concerns from an environmental viewpoint (Bai et al., 2014). Accordingly, there is a growing research interest pressed by governments and industries on the development of biodegradable and environmentally friendly materials. Poly(3-hydroxybutyrate) (PHB) is a fully biodegradable and biocompatible polyester synthesized by bacterial fermentation from renewable sources that has lately gained a lot of interest as a substitute to synthetic polymeric materials made from fossil fuels (Keshavarz & Roy, 2010). It is a non-toxic thermoplastic that comprises 3-hydroxy butyric acid units, [—O—CH—(CH_3)—CH_2—CO—]n, and can be now synthesized at an industrial level. PHB presents excellent biocompatibility and good stiffness due to its high crystallinity. However, its use has been limited owed to its brittleness, low impact resistance, moderately high water vapor permeability (WVP), and low degradation temperature (Mekonnen, Mussone, Khalil, & Bressler, 2013). To solve these drawbacks, the hydroxybutyrate units can be copolymerized with other monomers to achieve more flexibility, lower breakage, and reduced melting point. In particular, it can be polymerized with 3-hydroxyhexanoate units, which can be incorporated in PHB to obtain poly(3-hydroxybutyrateco-3-hydroxy-hexanoate) (PHBHHx), with chemical structure shown in Scheme 1.

This copolymer shows improved processability, higher ductility, and better impact strength (Diez-Pascual & Diez-Vicente, 2016). However, PHBHHx displays lower crystallinity than PHB, hence lower stiffness, and poorer barrier properties against moisture and gases, which is a shortcoming for its use as food packaging material. To increase its range of applications, strategies such as incorporation of nanofillers or polymer blending are pursued (Zhang, Liu, Mark, & Noda, 2009).

Zinc oxide (ZnO) nanostructures have recently attracted a lot of attention within the scientific community as future materials due to their inexpensiveness, easy availability, capability of performing surface modifications with different functional groups, and biocompatibility (Sirelkhatim et al., 2015). They also exhibit antimicrobial activity against human pathogen bacteria like *Staphylococcus aureus* even in the absence of light, and its effect is stronger than that reported for other metal oxides such as MgO, TiO_2, or CaO (Sawai, 2003). Further, they present strong UV absorption, therefore are extensively used in sensors, optical devices and antimicrobials. ZnO presents better antibacterial effect on *S. aureus* than other metal oxides like CuO or CeO_2 (Songfa et al., 2020). They are considered as non-toxic and do not induce damage to the DNA of human cells (Yamada, Suzuki, & Koizumi, 2007). They have been reported to be very effective for improving the barrier performance and antibacterial properties of polymers such as poly(phenylene sulphide) (Diez-Pascual & Diez-Vicente, 2014a), PHB (Diez-Pascual & Diez-Vicente, 2014b), and poly (3-hydroxybutyrate-co-3-hydroxyvalerate) (Diez-Pascual & Diez-Vicente, 2014c).

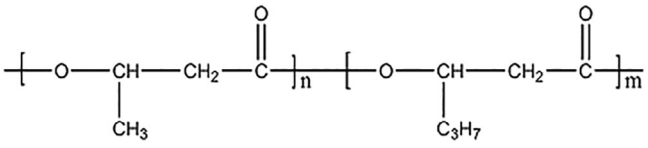

SCHEME 1 Chemical structure of poly(3-hydroxybutyrate-co-3-hydroxy-hexanoate (PHBHHx)

This study focuses on the preparation of ZnO-reinforced PHBHHx bionanocomposites incorporating 0.5, 1.0, 2.0, and 5.0 wt% nanoparticle loading by simple solution casting technique, and the analysis of their morphology, mechanical, thermal, barrier, and antibacterial properties with the aim to use them for food packaging applications.

2 | MATERIALS AND METHODS

2.1 | Materials

Poly(3-hydroxybutyrate-co-3-hydroxyhexanoate), PHBHHx, (M_n = 440,000 g/mol; T_g = 2°C, T_m = 110°C, $d_{25°C}$ = 1.25 g/cm^3, HHx = 12 mol%) was provided by Procter and Gamble Co (Cincinnati, OH , USA). The copolyester was purified by dissolution in hot chloroform, precipitation in methanol and drying under vacuum at 70°C for 24 hr. Zinc oxide nanopowder, <100 nm particle size and specific surface area in the range of 15–25 m^2/g, was provided by Sigma-Aldrich.

2.2 | Method

2.2.1 | Preparation of the nanocomposites

The nanocomposites with ZnO contents in the range of 0.5–5.0 wt% were prepared via ultrasonication followed by solution casting. The required amount of ZnO was dispersed in chloroform by ultrasonication at 100 W for 30 min. Subsequently, the PHBHHx was dissolved at 50°C in the nanoparticle dispersion and the mixture was sonicated for another 30 min. The resulting blend was poured into a glass Petri dish and finally dried under vacuum for 48 hr to remove the residual solvent.

2.2.2 | Transmission electron microscopy (TEM)

The morphology was studied by TEM using a Philips Tecnai 20 FEG (LaB_6 filament) microscope fitted with an Energy Dispersive X-Ray (EDX) detector, operating at 200 kV and with 0.3 nm point-to-point resolution. Ultra-thin sections of the composites were cut using a diamond knife and a Reichert Ultracut-S ultramicrotome equipped with a FCS cryo-device and placed onto copper grids.

2.2.3 | Water uptake (WU)

To calculate the WU, samples were dried in a desiccator at 0% relative humidity (RH) for 1 week. Then, they were placed in a beaker at 100% RH and absorbed water until a constant weight was reached. Water uptake was calculated according to the equation:

$$\mathrm{WU}\,(\%) = [(W_f - W_i)/W_i] \times 100 \quad (1)$$

where W_i and W_f are the initial and final weight of the samples, respectively. Five replicates for each sample were measured, using high-precision analytical balances (±0.001 g), and the average value is reported.

2.2.4 | Water vapor permeability (WVP)

The WVP was measured at 25°C following the gravimetric method ASTM E96-95 standard with Payne permeability cups. WVP was calculated according to the equation:

$$\mathrm{WVP} = (\Delta m \times l)/(A \times t \times \Delta P) \quad (2)$$

where Δm is the weight loss of each cup, l the film thickness, A the contact area, t the time, and ΔP the partial pressure difference between inside and outside of the cup.

2.2.5 | Oxygen permeability (OP)

The OP was evaluated at 25°C on films equilibrated at 54% RH by measuring the oxygen transference rate (OTR) with a gas permeability tester following the ASTM D3985-05 standard. OP was calculated as:

$$\mathrm{OP} = (\mathrm{OTR} \times l)/\Delta P \quad (3)$$

where l is the average film thickness and ΔP the difference between oxygen partial pressure across the film.

2.2.6 | Solubility tests

The solubility of film samples was tested at room temperature. Each sample was placed in a glass-weighing vessel, weighed, and covered with 30 ml of the corresponding solvent. After 90 min dissolution time, the non-dissolved fraction was separated by filtration, dried on filter paper until constant mass, and weighed.

2.2.7 | Tensile tests

Tensile properties were measured on an Instron tester following the ASTM D 638-03 standard, at a speed of 1 mm/min and a load cell of 100 kN, at 25°C and 50% RH. Six specimens for each type of nanocomposite were tested.

2.2.8 | Impact strength

Charpy notched impact strength tests were performed using a CEAST Fractovis dart impact tester on notched specimen bars, according to the ASTM D 6110-10 standard, at 25°C and 50% RH. Seven specimens were tested to get an average value.

2.2.9 | Fourier-transformed infrared spectroscopy

Attenuated total reflectance FT-IR spectra were recorded at room temperature on a Perkin-Elmer Spectrum One spectrometer equipped with a Universal ATR sampling accessory (diamond crystal) and a red laser excitation source (632.8 nm).

2.2.10 | Thermal stability

The thermal stability of the samples under a nitrogen atmosphere was measured by thermogravimetric analysis with a TA Instruments Q50 thermobalance. Samples were dried overnight and subsequently heated from room temperature to 550°C at a rate of 10°C/min.

2.2.11 | Antibacterial activity

Antibacterial action was tested against two pathogen bacteria: *S. aureus* (ATCC 12600) and *Escherichia coli* (ATCC 25922). After sterilization, the samples were submerged in a 3-day-old nutrient broth of ~2.0 × 106 colony forming units per ml (CFU/ml). After incubation at 37°C for 24 hr, the number of viable bacteria colonies was counted. The survival ratio (SR) was calculated as:

$$\mathrm{SR} = (N/N_o) \times 100 \quad (4)$$

where N_o and N are the average number of bacteria on the pure PHBHHx and the nanocomposites, respectively.

3 | RESULTS AND DISCUSSION

3.1 | Morphology of the nanocomposites

Morphology and crystallinity can play a substantial role in determining a packaging's vapor barrier properties. Thus, TEM analysis was carried out to investigate the morphology and state of dispersion of the nanoparticles within the matrix. Figure 1 presents typical TEM images of PHBHHx/ZnO nanocomposites with 0.5 (a) and 5.0 wt% ZnO (b).

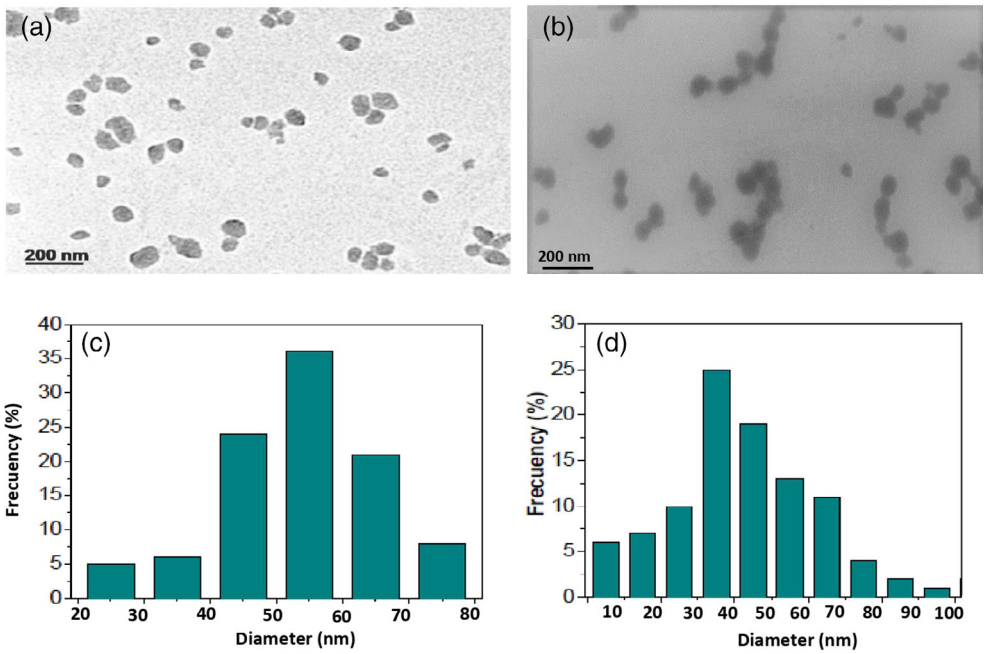

FIGURE 1 TEM images of PHBHHx/ZnO nanocomposites: (a) 0.5 wt%. (b) 5.0 wt%. (c) Particle diameter in 0.5 wt%. (d) Particle diameter in 5.0 wt%. PHBHHx, poly (3-hydroxybutyrate-co-3-hydroxy-hexanoate; ZnO, Zinc oxide

The micrograph in (a) reveals quasi-spherical nanoparticles randomly and well distributed within the polyester, without forming agglomerates. They show a quite narrow size distribution (Figure 1c), with diameters in the range of 20–80 nm and a mean value of 52 nm. Further, the nanofillers are quite regularly spaced, showing an average particle-particle distance of 160 nm. Nonetheless, at 5.0 wt% loading (Figure 1d), the nanoparticle dispersion is poorer. The size distribution is much wider, while the average nanoparticle size is similar. However, it was found that the average interparticle distance decreases, resulting in higher tendency toward aggregation, since the surface hydroxyl groups of ZnO have a strong tendency to create hydrogen bonds among nanoparticles, hence flocculation of the nanofillers can occur, causing the formation of small clusters. Overall, morphological analysis confirms that the dispersion of low concentrations of ZnO in PHBHHX occurs as single particles while both individual particles and small clusters appear at higher loadings. ZnO dispersion within the biopolymer was attained without the use of particle surface treatments or compatilibizing agents, making the fabrication process of these nanocomposites faster, cheaper, and more environmentally friendly.

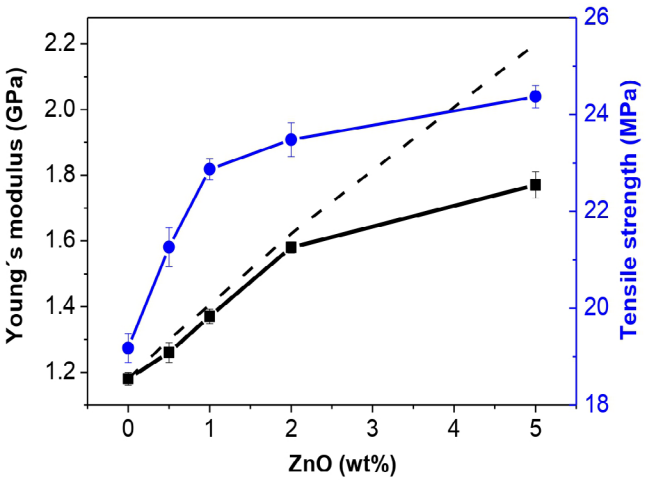

FIGURE 2 Young's modulus and tensile strength of PHBHHx/ZnO nanocomposites. The dashed lines correspond to the predictions according to the Krenchel's rule of mixtures (Equation (5)). PHBHHx, poly(3-hydroxybutyrate-co-3-hydroxy-hexanoate; ZnO, Zinc oxide

3.2 | Tensile properties

The room temperature static mechanical properties were evaluated by tensile tests, and the values of Young's modulus (E) and tensile strength (σ_y) derived from the stress–strain curves are depicted in Figure 2. The neat polymer exhibits a Young's modulus close to 1.2 GPa. The addition of ZnO nanoparticles results in a gradual increase in E, the highest rise being about 41% at 5.0 wt% loading. This extraordinary increment is attributed to the strong ZnO-polymer interfacial adhesion via hydrogen bonding interactions between the —OH groups of the ZnO surface and the ether and ester groups of the biopolymer. Similarly, the tensile strength increases from about 19.5 MPa up to 24.7 (about 27%) at 5.0 wt% loading. This increase is comparable to that reported for the same biopolymer covalently grafted to silane modified kaolinite/silica nanoparticles (Zhang et al., 2009), with the advantage that no chemical reactions were required in our study nor the use of silane compatibilizing agents. In contrast, no improvements in mechanical properties have been found upon incorporation of silk fibroin (Yang, Sun, Zhang, & Zhou, 2011). Nonetheless, composites with 2.0 and 5.0 wt% ZnO display close σ_y values, indicating that the strength is leveling off, thus higher ZnO loadings will not result in greater property improvements.

Taking into account the reported Young's modulus for ZnO (Kucheyev, Bradby, Williams, Jagadish, & Swain, 2002), the theoretical E values for the nanocomposites were estimated by the Krenchel's rule of mixtures for discontinuous reinforcement (Diez-Pascual & Diez-Vicente, 2014c) which can be written as indicated in the following equation:

$$E_c = (\eta E_f - E_m) V_f + E_m \quad (5)$$

where E_c, E_f, and E_m are the tensile modulus of the composite, filler, and matrix, respectively, V_f the filler volume fraction and η the strengthening coefficient that is 0.2 for randomly oriented fillers. The results obtained with Equation (4) are plotted in Figure 2 as a dashed line. Experimental Young's moduli of nanocomposites with loadings ≤2.0 wt% are in very good agreement with the theoretical calculations (differences lower than 12%). Only the nanocomposite with 5.0 wt% ZnO shows theoretical values significantly higher than the experimental, likely due to the presence of small nanoparticles aggregates, as shown in Figure 1, which limit the stress transfer ability. In fact, the model assumes perfect nanoparticle dispersion and nanoparticle-polymer interfacial adhesion; however, the nanofillers are not individually dispersed but gathered in small agglomerates, and shear slippage can occur within the aggregates, which restricts the stress-transfer to the matrix.

3.3 | Impact strength

Materials used in food technology should be tough and with good impact resistance. Therefore, the impact strength of the nanocomposites was measured, and the results from Charpy notched impact strength measurements are plotted in Figure 3. Neat PHBHHx has about 25% crystallinity (Xu et al., 2002), which leads to certain inherent brittleness and moderate impact resistance. As can be observed, the impact strength drops gradually with increasing ZnO loading, leading to around 36% decrease at 5.0 wt%. This dependency of the impact strength on the ZnO concentration was already predicted from the analysis of the areas under the tensile curves, and the results obtained by the two techniques show very similar trend.

The shape, size, state of nanofiller dispersion, and its adhesion with the matrix have strong influence on the rate of energy absorption, hence the impact properties of polymer composites (Diez-Pascual et al., 2010). On the one hand, the strong interfacial adhesion between the nanofiller and the matrix via H-bonding should provide an effective barrier for the advancing cracks, thus improving the impact strength. On the other hand, the nanofillers obstruct the ductile flow of the polymeric chains, hence leading to a reduction in ductility, which results in lower impact strength. Further, in the nanocomposite with the highest ZnO loading, the presence of small nanoparticle agglomerates might nucleate a few cracks, leading to a ductility reduction. Overall, the reduction in ductility prevails, which is reflected in lower impact strength values for the nanocomposites.

3.4 | Barrier properties

A key issue in food packaging is that of permeability. One of the foremost objectives when adding nanofillers to biopolymers is to improve their barrier properties against gases and vapors. Water vapor and oxygen are the two permeants most widely investigated in food packaging applications (Diez-Pascual & Diez-Vicente, 2014b). The water uptake and WVP of the developed nanocomposites are shown in Figure 4. Both parameters fall with increasing ZnO content, by a maximum of 68 and 45% at 5.0 wt% loading, which demonstrates better barrier properties for the nanocomposites, likely associated to their presence of the nanoparticles well dispersed within the matrix that increase the tortuosity of the transport path. Similar behavior of barrier performance improvement has been found for PHB filled with

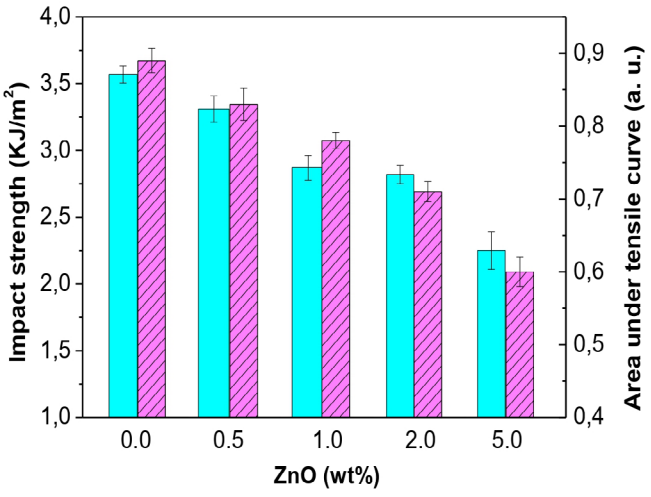

FIGURE 3 Charpy impact strength (solid bars) and area under the tensile curve (dashed bars) as a function of ZnO content. ZnO, Zinc oxide

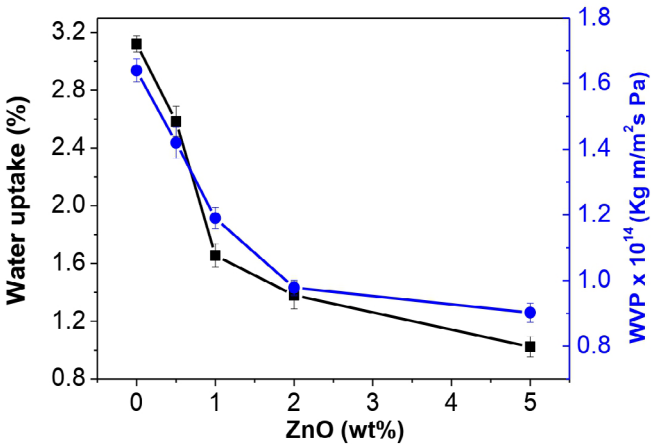

FIGURE 4 Water uptake (squares) and water vapor permeability (WVP, circles) versus ZnO loading. ZnO, Zinc oxide

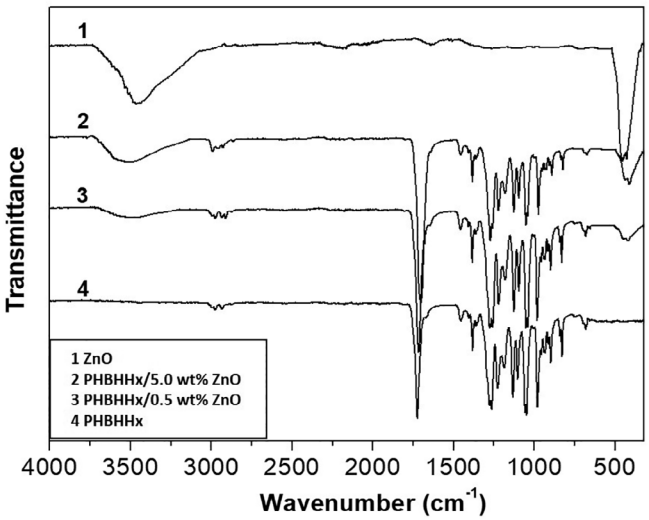

FIGURE 5 FT-IR spectra of neat PHBHHx, ZnO, and the nanocomposites with 0.5 and 5.0 wt% ZnO. FTIR, Fourier-transformed infrared spectroscopy; PHBHHx, poly (3-hydroxybutyrate-co-3-hydroxy-hexanoate; ZnO, Zinc oxide

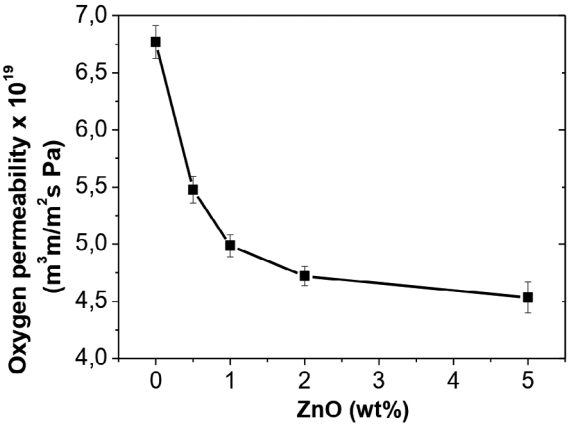

FIGURE 6 Oxygen permeability of PHBHHx/ZnO nanocomposites versus ZnO loading. PHBHHx, poly (3-hydroxybutyrate-co-3-hydroxy-hexanoate; ZnO, Zinc oxide

cellulose nanocrystals (Zhang et al., 2019), indicating that the resistance of the composite film to water and water vapor penetration has increased by the nanometer size effect of ZnO. Further, due to the hydrogen bonding between ZnO and PHBHHx in the composite film (Figure 5), a physical crosslinked network could be formed in the system, where the gas penetration becomes more difficult.

To corroborate the hydrogen bond formation, FT-IR analysis was performed on the different samples, and typical spectra of ZnO, PHBHHx and the nanocomposites with 0.5 and 5.0 wt% are shown in Figure 5. PHBHHx has a very strong band at 1725 cm^{-1} arising from the C═O stretching of the ester group. ZnO shows a wide peak around 3500 cm^{-1} due to the O—H stretching of hydrogen-bonded hydroxyl groups on the nanoparticle surface. In the nanocomposites, the same bands are observed, though the C═O stretching appears at a lower wavenumber, at around 10 and 30 cm^{-1} lower than that of neat PHBHHx for 0.5 and 5.0 wt% loading, respectively, indicative of hydrogen bond formation with the hydroxyl groups of the nanoparticles.

Regarding the oxygen permeability of the nanocomposites (Figure 6), a clear reduction is also observed as the ZnO content rises, presenting a minimum (about 35% decrement as compared to neat PHBHHx) at the highest nanofiller concentration.

This improved barrier performance should be related to the strong ZnO-polymer interfacial adhesion that causes chain immobilization. Further, it has been demonstrated that ZnO nanoparticles reduce the oxygen permeability of polymer nanocomposites not only by creating a tortuous path but also via gas adsorption onto their surface (Elen et al., 2012). Thus, the higher the ZnO loading, the higher the level of tortuosity. On the other hand, the presence of nanofiller aggregates in the nanocomposite with 5.0 wt% could result in the formation of favored paths for the permeants to diffuse more rapidly, hence reduced barrier performance. Overall, it seems that the increase in the level of tortuosity outweighs the presence of nanofiller aggregates; hence, the oxygen permeability of the nanocomposite with 5.0 wt% ZnO is slightly lower than that with 2.0 wt% loading. Similar trend has been reported for PHB/ZnO nanocomposites (Diez-Pascual & Diez-Vicente, 2014b), where 5.0 wt % ZnO was the optimal nanofiller concentration. Results prove that the incorporation of ZnO to PHBHHx matrix has a beneficial effect on the gas barrier properties, rendering improved materials for packaging oxygen- and/or moisture-sensitive products.

With a view to use the developed nanocomposites for food packaging, it is interesting to investigate their solvent resistance. Hence, solubility tests were carried out of neat PHBHHx and the different nanocomposites, and the results are collected in Table 1. Neat PHBHHx is insoluble in water and high polar solvents like methanol or ethanol, and the same applies to the nanocomposites. This is consistent with the results from water uptake measurements (Figure 4). However, it is partly soluble in acetic acid and aniline, in agreement with results reported previously (Terada & Marchessault, 1999). The acid resistance hardly changes with increasing ZnO loading, whereas base resistance improves, which is reasonable considering that ZnO is soluble in acid but insoluble in base (Beşe, Borulu, Çopur, Çolak, & Ata, 2010).

On the other hand, all the samples are insoluble in non-polar solvents like hexane, while nanocomposites with low ZnO loading are soluble in halogenated polar solvents such as dichloromethane or chloroform. The solubility in polar protic solvents such as dimethylformamide (DMF) and acetone decreases with increasing ZnO content.

3.5 | Thermal stability

One main challenge of PHBHHx is its low thermal stability, as thermal degradation can take place during the polymer melt processing. Therefore, it is important to assess the effect of ZnO nanoparticles on

TABLE 1 Solubility of PHBHHx and the poly(3-hydroxybutyrate-co-3-hydroxy-hexanoate/Zinc oxide (PHBHHx/ZnO) nanocomposites in different solvents

Sample	Water (H_2O)	Dimethylformamide (DMF)	Aniline ($C_6H_5NH_2$)	Dichloromethane (CH_2Cl_2)	Chloromethane (CH_3Cl)
PHBHHx	I	S	PS	S	S
PHBHHx/0.5 ZnO	I	S	PS	S	S
PHBHHx/1.0 ZnO	I	S	PS	S	S
PHBHHx/2.0 ZnO	I	PS	I	S	S
PHBHHx/5.0 ZnO	I	PS	I	PS	PS
Sample	Acetone ($(CH_3)_2CO$)	Acetic acid (CH_3COOH)	Hexane (C_6H_{14})	Methanol (CH_3OH)	Ethanol (CH_3CH_2OH)
PHBHHx	PS	PS	I	I	I
PHBHHx/0.5 ZnO	I	PS	I	I	I
PHBHHx/1.0 ZnO	I	PS	I	I	I
PHBHHx/2.0 ZnO	I	PS	I	I	I
PHBHHx/5.0 ZnO	I	S	I	I	I

Abbreviations: I, insoluble; PS, partially soluble; S, soluble.

the decomposition of this biopolymer. Figure 7 shows the TGA and DTG curves of ZnO, PHBHHx, and the nanocomposites under a nitrogen atmosphere. As can be observed, the raw nanoparticles show a very small weight loss under 300°C probable due to the removal of physically and chemically adsorbed surface water. On the other hand, the neat polymer show a single decomposition step that starts at about 300°C and shows the maximum rate of weight loss at around 350°C. Similar behavior is found for the nanocomposites, though the curves are moved toward high temperatures, indicating stabilization due to the incorporation of the nanoparticles. Thus, the initial degradation temperature gradually increasing with increasing ZnO concentration, and the best stability is found for the composite with the higher loading. The uniform ZnO distribution within PHBHHx as revealed by TEM and the strong nanofiller–matrix interactions by hydrogen bonding (Figure 5) would create a barrier effect opposing the diffusion of the decomposition products from the interior of the matrix to the gas phase.

3.6 | Antibacterial activity

The antibacterial action of neat PHBHHx and the nanocomposites was explored against two model pathogen bacteria: *E. coli* (Gram-negative) and *S. aureus* (Gram-positive), and the results are shown in Figure 8. Clearly, the survival ratio of both bacteria decreases progressively upon raising ZnO content, and the greatest antibacterial activity (about 98 and 95% growth inhibition for *E. coli* and *S. aureus*,

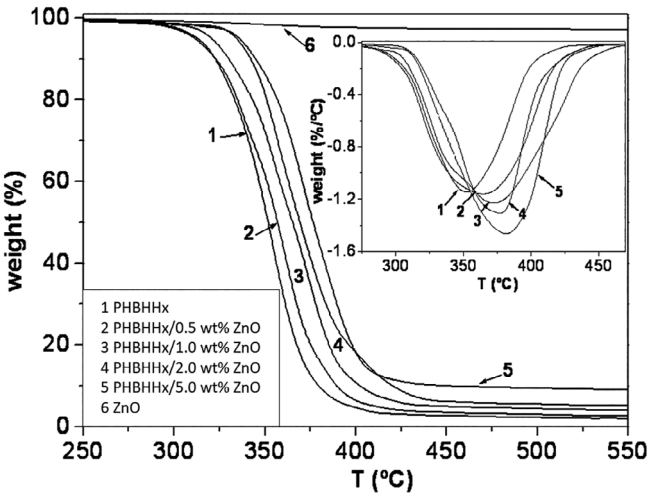

FIGURE 7 Themogravimetric curves (TGA) for neat PHBHHx and PHBHHx/ZnO nanocomposites under a nitrogen atmosphere. The inset shows the differential thermogravimetric curves (DTG). PHBHHx, poly(3-hydroxybutyrate-co-3-hydroxy-hexanoate; ZnO, Zinc oxide

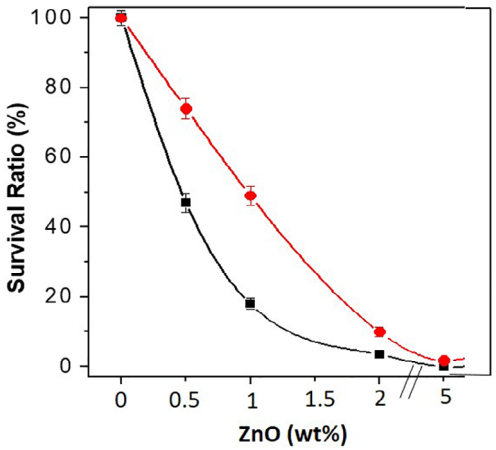

FIGURE 8 Effect of PHBHHx/ZnO nanocomposites on the survival ratio of *Escherichia coli* (solid squares) and *Staphylococcus aureus* (open circles). PHBHHx, poly(3-hydroxybutyrate-co-3-hydroxy-hexanoate; ZnO, Zinc oxide

respectively) is obtained at the highest ZnO loading (5.0 wt%). The biocide effect on *E. coli* is steadily greater than on *S. aureus*, which is consistent with previous studies (Liu & Yang, 2003) that reported more effective action of ZnO nanoparticles against Gram-negative bacteria. The differences between the two types of bacteria are likely due to structural and chemical compositional differences of the cell surfaces. Thus, Gram-positive bacteria have a single cytoplasmic membrane and a thick wall comprising peptidoglycan layers, whereas the Gram-negative have a more complex cell wall, with a layer of peptidoglycan between the outer membrane and the cytoplasmic membrane. Despite the mechanism of action is not clear yet, it is likely due to the production of H_2O_2 from the ZnO surface. The nanoparticles lead an increase in the formation of reactive oxygen species (ROS) that results into the destruction of the bacterial cells. These elevated ROS result in lipid peroxidation, which destroys the membrane integrity (Tiwari et al., 2018).

4 | CONCLUSION

The morphology, solvent resistance, mechanical, thermal, antibacterial, and barrier properties of novel ZnO-reinforced PHBHHx bionanocomposites prepared via ultrasonication followed by solution casting have been analyzed. TEM images revealed the presence of small ZnO agglomerates at 5.0 wt% loading, while samples with lower ZnO content showed nanoparticles randomly and individually distributed throughout the polymer matrix. The addition of the nanoparticles enhanced the stiffness and strength of the biopolymer, by up to 41 and 27% at 5.0 wt% concentration, while decreased the impact strength due to the reduction in the matrix ductility. Further, it improved the barrier properties of the biopolymer, decreasing the water uptake, water vapor permeability, and oxygen permeability (by about 68, 45, and 35% decrement at 5.0 wt% loading), attributed to the strong matrix–ZnO interactions via H-bonding. Improved resistance against polar protic solvents such as DMF or acetone was also found. Moreover, an outstanding rise in the thermal stability of the biopolymer was observed. Antimicrobial tests demonstrate the great potential of the developed nanocomposites to prevent microbial contamination. PHBHHx/ZnO bionanocomposites, in particular that with 5.0 wt% ZnO concentration, are an interesting alternative to petroleum-based polymeric materials for use in a variety of food packaging applications.

ACKNOWLEDGMENT

Action financed by the Community of Madrid within the framework of the multi-year agreement with the University of Alcalá in the line of action "Stimulus to Excellence for University Permanent Professors," ref. EPU-INV/2020/012.

AUTHOR CONTRIBUTIONS

Ana Maria Diez Pascual: Conceptualization; data curation; formal analysis; funding acquisition; investigation; project administration; writing - original draft; writing-review & editing.

DATA AVAILABILITY STATEMENT

The author confirms that the data supporting the findings of this study are available within the article .

ORCID

Ana M. Díez-Pascual https://orcid.org/0000-0001-7405-2354

REFERENCES

Bai, H., Huang, C., Xiu, H., Zhang, Q., Deng, H., Wang, K., & Fu, Q. (2014). Significantly improving oxygen barrier properties of polylactide via constructing parallel-aligned shish-kebab-like crystals with well-interlocked boundaries. *Biomacromolecules*, *15*, 1507–1514. https://doi.org/10.1021/bm500167u

Beşe, A., Borulu, N., Çopur, M., Çolak, S., & Ata, O. (2010). Optimization of dissolution of Zn and Cd metals from Waelz sintering waste by hydrochloric acid solutions. *Chemical Engineering Journal*, *162*, 718–722. https://doi.org/10.1016/j.cej.2010.06.035

Diez-Pascual, A. M., & Diez-Vicente, A. L. (2014a). High-performance aminated poly(phenylene sulfide)/ZnO nanocomposites for medical applications. *ACS Applied Materials and Interfaces*, *6*, 10132–10145. https://doi.org/10.1021/am501610p

Diez-Pascual, A. M., & Diez-Vicente, A. L. (2014b). Poly (3-hydroxybutyrate)/ZnO bionanocomposites with improved mechanical, barrier and antibacterial properties. *International Journal of Molecular Science*, *15*, 10950–10973. https://doi.org/10.3390/ijms150610950

Diez-Pascual, A. M., & Diez-Vicente, A. L. (2014c). ZnO-reinforced poly (3-hydroxybutyrate-co-3-hydroxyvalerate) bionanocomposites with antimicrobial function for food packaging. *ACS Applied Materials and Interfaces*, *6*, 9822–9834. https://doi.org/10.1021/am502261e

Diez-Pascual, A. M., & Diez-Vicente, A. L. (2016). Electrospun fibers of chitosan-grafted polycaprolactone/poly(3-hydroxybutyrate-co-3-hydroxyhexanoate) blends. *Journal of Materials Chemistry B*, *4*, 600–612. https://doi.org/10.1039/C5TB01861G

Diez-Pascual, A. M., Naffakh, M., Gonzalez-Domínguez, J. M., Anson, A., Martinez-Rubi, Y., Martinez, M. T., … Gomez, M. A. (2010). High performance PEEK/carbon nanotube composites compatibilized with polysulfones-I. Structure and thermal properties. *Carbon*, *48*, 3485–3499. https://doi.org/10.1016/j.carbon.2010.05.046

Elen, K., Murariu, M., Peeters, R., Dubois, P., Mullens, J., Hardy, A., & van Bael, M. K. (2012). Towards high-performance biopackaging: Barrier and mechanical properties of dual-action polycaprolactone/zinc oxide nanocomposites. *Polymers Advances and Technology*, *23*, 1422–1428. https://doi.org/10.1002/pat.2062

Keshavarz, T., & Roy, I. (2010). Polyhydroxyalkanoates: Bioplastics with a green agenda. *Current Opinion Microbiology*, *13*, 321–326. https://doi.org/10.1016/j.mib.2010.02.006

Kucheyev, S. O., Bradby, J. E., Williams, J. S., Jagadish, C., & Swain, M. V. (2002). Mechanical deformation of single-crystal ZnO. *Applied Physical Letters*, *80*, 956–958. https://doi.org/10.1063/1.1448175

Liu, H. L., & Yang, T. C. K. (2003). Photocatalytic inactivation of *Escherichia coli* and *Lactobacillus helveticus* by ZnO and TiO_2 activated with ultraviolet light. *Process Biochemistry*, *39*, 475–481. https://doi.org/10.1016/S0032-9592(03)00084-0

Mekonnen, T., Mussone, P., Khalil, H., & Bressler, D. (2013). Progress in bio-based plasctics and plasticizing modifications. *Journal of Materials Chemistry A*, *1*, 13379–13398. https://doi.org/10.1039/C3TA12555F

Sawai, J. (2003). Quantitative evaluation of antibacterial activities of metallic oxide powders (ZnO, MgO and CaO) by conductimetric assay. *Journal of Microbiological Methods*, *54*, 177–182. https://doi.org/10.1016/S0167-7012(03)00037-X

Sirelkhatim, A., Mahmud, S., Seeni, A., Kaus, N., Ann, L. C., Bakhori, S., … Mohamad, D. (2015). Review on zinc oxide nanoparticles: Antibacterial

activity and toxicity mechanism. *Nano-micro Letters*, *7*, 219–242. https://doi.org/10.1007/s40820-015-0040-x

Songfa, Q., Hong, Z., Zhichuan, S., Li, H., Huayao, C., & Xinhua, Z. (2020). Synthesis, characterization, and comparison of antibacterial effects and elucidating the mechanism of ZnO, CuO and CuZnO nanoparticles supported on mesoporous silica SBA-3. *RSC Advances*, *10*, 2767–2785. https://doi.org/10.1039/C9RA09829A

Terada, M., & Marchessault, R. H. (1999). Determination of solubility parameters for poly(3-hydroxyalkanoates). *International Journal of Biological Macromolecules*, *25*, 207–215. https://doi.org/10.1016/s0141-8130(99)00036-7

Tiwari, V., Mishra, N., Gadani, K., Solanki, P. S., Shah, N. A., & Tiwari, M. (2018). Mechanism of anti-bacterial activity of zinc oxide nanoparticle against Carbapenem-resistant *Acinetobacter baumannii*. *Frontiers in Microbiology*, *9*, 1218. https://doi.org/10.3389/fmicb.2018.01218

Xu, J., Guo, B.-H., Yang, R., Wu, Q., Chen, G.-Q., & Zhang, Z.-M. (2002). In situ FTIR study on melting and crystallization of polyhydroxyalkanoates. *Polymer*, *43*, 6893–6899. https://doi.org/10.1016/S0032-3861(02)00615-8

Yamada, H., Suzuki, K., & Koizumi, S. (2007). Gene expression profile in human cells exposed to zinc. *Journal of Toxicological Science*, *32*, 193–196. https://doi.org/10.2131/jts.32.193

Yang, H.-X., Sun, M., Zhang, Y., & Zhou, P. (2011). Degradable PHBHHx modified by the silk fibroin for the applications of cardiovascular tissue engineering. *International Scholarly Research Notices*, *2011*, 389872. https://doi.org/10.5402/2011/389872

Zhang, B., Huang, C., Zhao, H., Wang, J., Yin, C., Zhang, L., & Zhao, Y. (2019). Effects of cellulose nanocrystals and cellulose nanofibers on the structure and properties of Polyhydroxybutyrate nanocomposites. *Polymers*, *11*, 2063. https://doi.org/10.3390/polym11122063

Zhang, Q., Liu, Q., Mark, J. E., & Noda, I. (2009). A novel biodegradable nanocomposite based on poly(3-hydroxybutyrate-co-3-hydroxyhexanoate) and silylated kaolinite/silica core-shell nanoparticles. *Applied Clay Science*, *46*, 51–56. https://doi.org/10.1016/j.clay.2009.07.008

How to cite this article: Díez-Pascual, A. M. (2021). Poly(3-hydroxybutyrate-co-3-hydroxyhexanoate) with zinc oxide nanoparticles for food packaging. *Journal of Food Process Engineering*, e13814. https://doi.org/10.1111/jfpe.13814